Strain–driven endohedral redox couple CeIV/CeIII in nitride clusterfullerenes CeM2N@C80 (M = Sc, Y, Lu)

ARTICLE *in* JOURNAL OF PHYSICAL CHEMISTRY LETTERS · JULY 2013

Impact Factor: 7.46 · DOI: 10.1021/jz4009773

4 AUTHORS, INCLUDING:

Alexey A Popov

Leibniz Institute for Solid State and Materials …

188 PUBLICATIONS **3,412** CITATIONS

SEE PROFILE

THE JOURNAL OF PHYSICAL CHEMISTRY Letters

Letter

pubs.acs.org/JPCL

Strain-Driven Endohedral Redox Couple Ce^{IV}/Ce^{III} in Nitride Clusterfullerenes $CeM_2N@C_{80}$ (M = Sc, Y, Lu)

Yang Zhang, Sandra Schiemenz, Alexey A. Popov,* and Lothar Dunsch*

Department of Electrochemistry and Conducting Polymers, Leibniz-Institute for Solid State and Materials Research (IFW) Dresden, D-101171 Dresden, Germany

Supporting Information

ABSTRACT: Electrochemical and NMR spectroscopic studies prove the endohedral oxidation of Ce^{III} in nitride clusterfullerenes $CeM_2N@C_{80}$ (M = Sc, Y, Lu). The redox potential of the endohedral Ce^{IV}/Ce^{III} couple systematically varies with the ionic radius of the second cluster metal. DFT computations show that this metal dependence is caused by the release of strain when Ce^{IV} with a small ionic radius is formed. In particular, after endohedral oxidation the pyramidal CeY_2N cluster becomes planar in the $[CeM_2N@C_{80}]^+$ cation.

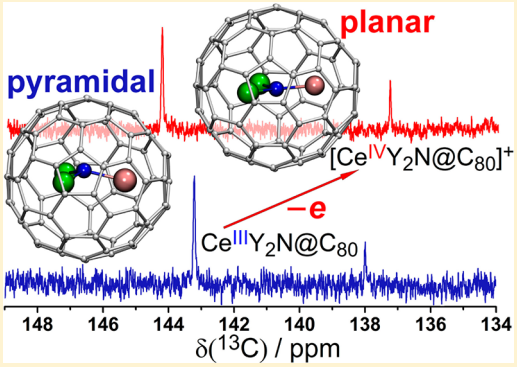

SECTION: Physical Processes in Nanomaterials and Nanostructures

Endohedral fullerenes (EMFs) stand for a unique form of fullerenes with atoms, clusters, or molecules encapsulated in their interior space.[1−5] Recently, it was established that not only unusual species can be stabilized inside of the fullerene cages but also that the spin and charge states of such species can be manipulated by endohedral redox processes.[6−11] The studies of such processes, in which a carbon cage acts as a redox-inert but electron-transparent container, constitute the recently emerged discipline known as *endohedral electrochemistry*.[6] The family of nitride clusterfullerenes (NCFs) $M_3N@C_{2n}$[12,13] provides an especially convenient platform for creation and tuning of endohedrally redox-active species. Whereas the M_3N cluster remains redox-inert in a majority of NCFs ($Sc_3N@C_{80}$ is a notable exception),[14−17] it is possible to use the nitride cluster as a matrix to introduce an electroactive metal in the form of the mixed metal NCFs. For instance, both oxidation and reduction of $TiM_2N@C_{80}$ (M = Sc, Y) proceed through a change of the valence state of the Ti atom.[9,10] The redox behavior of endohedral Ce is another exquisite example of the special role of the mixed metal nitride cluster. Whereas the Ce^{III} state in $Ce_2@C_{72,78,80}$,[18−21] $Ce@C_{82}$,[22] or $Ce_3N@C_{88,92,96}$[23,24] remains unaffected by the electrochemical oxidation of the EMF molecules, an unprecedented negative shift of the oxidation potential of $CeLu_2N@C_{80}$ in comparison to the standard values of $M_3N@C_{80}$ NCFs was discovered and tentatively assigned to the endohedral oxidation of Ce^{III} to Ce^{IV}.[11] Remarkably, examples of the Ce^{IV}/Ce^{III} redox couple in organolanthanide chemistry are rather scarce[25] (e.g., $Ce(C_8H_8)_2$,[26] $Ce(Cp)_3(O\text{-}i\text{-}Pr)$,[27] Ce(octaethylporphyrin)$_2$,[28] Ce complexes in the heterobimetallic framework[29]), and finding such a couple in EMF opens a new dimension in organocerium chemistry.[30] In this Letter, we report the synthesis of $CeY_2N@C_{80}$, provide compelling evidence of the endohedral oxidation of Ce^{III} in $CeM_2N@C_{80}$ (M = Sc, Y, Lu), and show that the redox potential of the Ce^{IV}/Ce^{III} couple in the CeM_2N cluster systematically varies with the cluster size as a result of the inner strain.

Synthesis and NMR Spectra of Pristine Clusterfullerenes. $CeY_2N@C_{80}$ (isomer I; hereafter, the label for the isomeric structure is omitted) was synthesized by the "selective organic solid" route using guanidine thiocyanate as the nitrogen source[31] and isolated by a two-step HPLC procedure; further details are described in the Supporting Information (SI). $CeSc_2N@C_{80}$ (first reported by Dorn et al.[32]) and $PrSc_2N@C_{80}$ were obtained in a similar procedure; ∼1 mg of each EMF was accumulated for the present study. On the basis of HPLC data, the relative yield of $CeY_2N@C_{80}$ is ∼10 times smaller than that of $CeSc_2N@C_{80}$. The vis−NIR absorption spectra of $CeM_2N@C_{80}$ (M = Sc, Lu, Y) are almost identical and exhibit only subtle shifts of the wavelengths (see the SI). The spectra are also similar to those of many other $M_3N@C_{80}$ with the $I_h(7)$ carbon cage and show that electronic properties of $CeM_2N@C_{80}$ are not significantly altered by the $4f^1$ electron of Ce or switching of the second metal.

The 125 MHz ^{13}C NMR spectra of $CeM_2N@C_{80}$ (M = Sc, Lu, Y) obtained at 288 K exhibit two peaks with a 3:1 intensity ratio (Figure 1), which unambiguously proves the $I_h(7)$

Received: May 10, 2013
Accepted: July 7, 2013
Published: July 8, 2013

   dx.doi.org/10.1021/jz4009773 | J. Phys. Chem. Lett. 2013, 4, 2404−2409

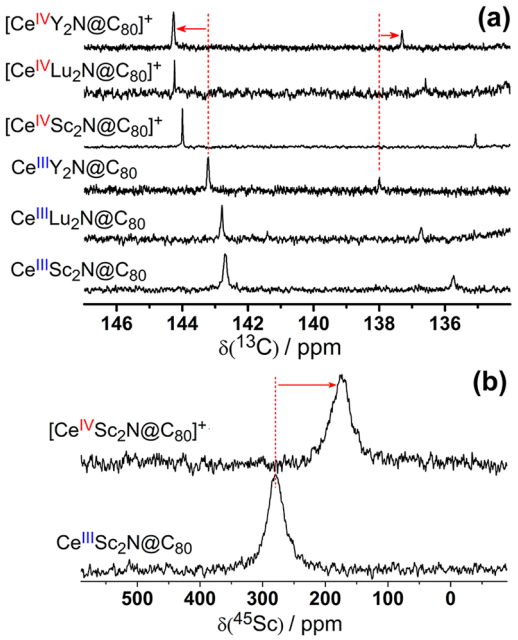

Figure 1. (a) ^{13}C NMR spectra of paramagnetic $Ce^{III}M_2N@C_{80}$ (M = Sc, Y and Lu) and their oxidized diamagnetic counterparts $[Ce^{IV}M_2N@C_{80}]^+$ measured in *o*-d_4-DCB at 288 K; (b) ^{45}Sc NMR spectra of $CeSc_2N@C_{80}$ and $[CeSc_2N@C_{80}]^+$.

symmetry of the carbon cage and a rapid rotation of the CeM_2N cluster.[13,33] Compared to the typical $\delta(^{13}C)$ values in diamagnetic $M_3N@C_{80}$-$I_h(7)$,[33] the ^{13}C NMR signals in $CeM_2N@C_{80}$ experience a paramagnetic shift of 1−3 ppm due to the Ce^{III}-$4f^1$ electron. The relatively small values of such shifts are ascribed to averaging over the whole carbon cage because of the rotation of the cluster. Variable-temperature studies in the 268−308 K range revealed a pronounced temperature dependence of the $\delta(^{13}C)$ values. In agreement with earlier ^{13}C NMR studies of Ce-EMFs,[8,18,20,21] the main contribution to paramagnetic shift was assigned to the pseudocontact term, δ_{pc}, which scales with temperature as $c_{pc}\cdot T^{-2}$ (c_{pc} is a characteristic constant for each kind of ^{13}C nuclei in the molecule). Extrapolation of the dependence $\delta(T) = \delta_{dia} + c_{pc}\cdot T^{-2}$ to the $T^{-2}= 0$ limit gave the values of the diamagnetic contributions, δ_{dia}, and c_{pc} constants listed in Table 1. Extrapolated δ_{dia} shifts are in the range of the $\delta(^{13}C)$ shifts found for diamagnetic $M_3N@C_{80}$ NCFs, thus confirming the prevalence of the pseudocontact term. The c_{pc} constants of $\sim -0.2 \times 10^6$ K^2 are comparable to the values in $Ce_2@C_{80}$-$I_h(7)$ with freely circulating Ce atoms[18] and are significantly smaller than c_{pc} constants in Ce-EMFs with more restricted motion ($Ce_2@C_{80}$-D_{5h}[18]) or localized position of Ce atoms ($Ce_2@C_{72}$[21] or $Ce_2@C_{78}$[20]).

Another remarkable feature of the ^{13}C NMR spectra of $CeM_2N@C_{80}$ is the systematic variation of the chemical shifts that depends on the second metal in the cluster. With the increase of the ionic radius of M^{3+} in the Sc^{3+} (0.75 Å) → Lu^{3+} (0.85 Å) → Y^{3+} (0.90 Å) series,[34] both ^{13}C NMR signals of the fullerene cage shift upfield. The shift is especially pronounced for the higher-field signal, corresponding to the carbon atoms on triple-hexagon junctions (THJ, also known as pyrene-type atoms). Such a metal size dependence agrees well with the results of our former studies of ^{13}C NMR spectra in a series of $Sc_xLu_{3-x}N@C_{80}$ and $Y_xLu_{3-x}N@C_{80}$ (x = 0−3), which showed a similar dependence on the ionic radii of the metals.[33] These studies showed that the change of the cluster size increases the pyramidalization of the metal-coordinated carbon atoms, and the effect is more pronounced for the THJ atoms. In due turn, a perfect linear correlation between pyramidalization of the carbon atoms (quantified in terms of the π-orbital axis vector analysis[35]) and $\delta(^{13}C)$ was established. Figure 1 shows that the same reasoning applies also to $CeM_2N@C_{80}$. Paramagnetism of Ce^{III} and the cluster-induced pyramidalization of the carbon atoms impose a similar influence on the $\delta(^{13}C)$ values on the order of a few ppm, and their exact contributions cannot be discerned at this moment.

Electrochemical Studies. The results of electrochemical studies of $CeM_2N@C_{80}$ NCFs performed in *o*-DCB are shown in Figure 2 and summarized in Table 2. In the cathodic range, all

Table 1. ^{13}C NMR Chemical Shifts in $CeM_2N@C_{80}$-$I_h(7)$[a]

	q = 0			q = +1
$CeM_2N@C_{80}$	δ, T = 288 K	c_{pc}[b] ×10^6 K^2	δ_{dia}	δ
$CeSc_2N@C_{80}$	142.69	−0.22	145.29	144.02
	135.74	−0.17	137.93	135.08
$CeLu_2N@C_{80}$	142.79	−0.20	144.85	144.24
	136.72	−0.23	139.06	136.59
$CeY_2N@C_{80}$	143.22	−0.17	145.38	144.27
	138.00	−0.24	140.92	137.31

[a]The data are given for the neutral state (q = 0) and the cationic state (q = +1). [b]c_{pc} and δ_{dia} are obtained in CS_2 solution in the 268−308 K range.

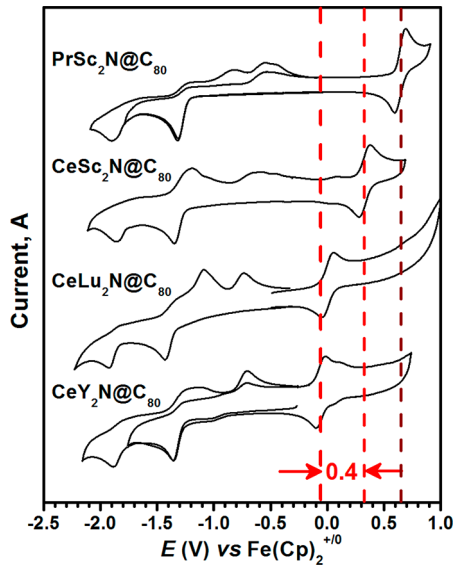

Figure 2. Cyclic voltammograms of $CeM_2N@C_{80}$ (M = Y, Lu and Sc) and $PrSc_2N@C_{80}$ measured in *o*-DCB solution with $TBABF_4$ as the supporting electrolyte; scan rate, 100 mV/s.

compounds exhibit two electrochemically irreversible one-electron reduction steps with peak potentials (E_p) near −1.36 and −1.92 V (all potentials hereafter are versus $Fc(Cp)_2^{+/0}$). Variation of the E_p values with different cluster composition did not exceed 0.1 V. This behavior is typical for $M_3N@C_{80}$ NCFs and is consistent with the carbon-cage-based reductions.[14,15,36,37] A drastically different situation is found in the anodic range. All $CeM_2N@C_{80}$ compounds exhibit a reversible one-electron oxidation step with strongly metal-dependent half-

dx.doi.org/10.1021/jz4009773 | J. Phys. Chem. Lett. 2013, 4, 2404−2409

Table 2. Redox Potentials of $CeM_2N@C_{80}$-$I_h(7)$ and $PrSc_2N@C_{80}$-$I_h(7)$[a]

NCF	method	ox $E_{1/2}$	red-I E_p	red-II E_p	gap_{EC}
$CeY_2N@C_{80}$	CV	−0.07	−1.36	−1.88	1.30
	SWV	−0.06	−1.32	−1.83	1.25
$CeLu_2N@C_{80}$	CV	0.01	−1.43	−1.92	1.44
	SWV	0.01	−1.39	−1.88	1.40
$CeSc_2N@C_{80}$	CV	0.33	−1.34	−1.87	1.67
	SWV	0.33	−1.31	−1.83	1.64
$PrSc_2N@C_{80}$	CV	0.64	−1.32	−1.91	1.96
	SWV	0.64	−1.26	−1.83	1.91

[a]All values in V versus $Fe(Cp)_2^{+/0}$ couple; CV denotes cyclic voltammetry, SWV is square-wave voltammetry, $E_{1/2}$ is the half-wave potential (for CV), and E_p is a peak potential.

wave potentials ($E_{1/2}$). The most negative $E_{1/2}$ value of −0.07 V is recorded for $CeY_2N@C_{80}$, followed by $CeLu_2N@C_{80}$ at 0.01 V and $CeSc_2N@C_{80}$ at 0.33 V. Thus, enlarging the size of the encaged CeM_2N cluster induces a large negative shift (up to 0.4 V) of the oxidation potential.

The large difference between the oxidation potential of $CeLu_2N@C_{80}$ and that of other $M_3N@C_{80}$ NCFs ($E_{1/2} \approx 0.6$–0.7 V) served as the first indication of the Ce-based redox process in $CeLu_2N@C_{80}$.[8] Likewise, the endohedral oxidation of Ce can be postulated for $CeY_2N@C_{80}$ studied in this work. A significantly more positive oxidation potential of $CeSc_2N@C_{80}$ raises the question whether it can be also assigned to the endohedral Ce^{IV}/Ce^{III} couple or if oxidation of the carbon cage takes place. For comparison, we have studied redox properties of $PrSc_2N@C_{80}$ as the closest analogue of $CeSc_2N@C_{80}$ with a similar size nitride cluster. Reversible oxidation of $PrSc_2N@C_{80}$ is found at +0.64 V, in close similarity to many other $M_3N@C_{80}$ molecules. The $E_{1/2}$(ox) difference of 0.31 V between $CeSc_2N@C_{80}$ and $PrSc_2N@C_{80}$ indicates that oxidation of $CeSc_2N@C_{80}$ is a Ce-based process.

NMR Spectra of Oxidized Ce-NCFs. Compelling evidence of the endohedral oxidation of Ce^{III} in all studied $CeM_2N@C_{80}$ NCFs is obtained by ^{13}C NMR spectroscopy. If the oxidation of $CeM_2N@C_{80}$ is a fullerene-based process, their radical cations are expected to give no measurable NMR spectra, whereas an endohedral $Ce^{III} \rightarrow Ce^{IV}$ oxidation produces diamagnetic cations accessible by ^{13}C NMR spectroscopy. $[CeM_2N@C_{80}]^+$ cations were obtained in *o*-DCB solution by reacting NCFs with $[Fe(Cp)_2]^+[BF_4]^-$ (M = Y) or $Ag^+[PF_6]^-$ (M = Sc, Lu).[38] The spectra measured after addition of the oxidation agent (Figure 1a) show a two-line pattern similar to that of $CeM_2N@C_{80}$, but the peaks are shifted to the lower field, closer to the chemical shifts of diamagnetic $M_3N@C_{80}$ NCFs and δ_{dia} values determined for $CeM_2N@C_{80}$ (Table 1). Furthermore, the peak at δ = 280 ppm in the ^{45}Sc NMR spectrum of $CeSc_2N@C_{80}$ is shifted to 175 ppm in $[CeSc_2N@C_{80}]^+[PF_6]^-$ (Figure 1b), which is close to the value of $\delta(^{45}Sc)$ = 190 ppm measured for $Sc_3N@C_{80}$ in *o*-DCB (note that ^{45}Sc chemical shifts in Sc-based endohedral fullerenes can vary in the range of several hundred ppm; see refs 1 and 7 for a discussion). Thus, NMR spectroscopy strongly supports that diamagnetic $[Ce^{IV}M_2N@C_{80}]^+$ cations are produced. This is the first NMR spectroscopic study of any NCF in the charged form.

DFT Computations. As far as the endohedral oxidation of Ce^{III} is confirmed, the question to be considered is why then the oxidation potential of the Ce^{III} in the CeM_2N cluster depends so strongly on the second cluster metal, M, which is not involved in the redox process. To address this problem, we have performed DFT PBE0/SVP calculations of the $CeM_2N@C_{80}$ and $M_3N@C_{80}$ molecules in the neutral and charged states using the Firefly package.[39] Table 3 lists

Table 3. DFT-Computed IPs and Bond Lengths in $CeM_2N@C_{80}$ and $M_3N@C_{80}$ (M = Sc, Lu, Y)[a]

NCF	IP_{Ce}	IP_{cage}	$d_{M-N}(0\rightarrow+1)$[b]	d_{Ce-N} $(0\rightarrow+1)$
$CeY_2N@C_{80}$	6.34	6.96	2.052 → 2.117	2.100 → 1.956
$Y_3N@C_{80}$		6.95	2.048	
$CeLu_2N@C_{80}$	6.50	6.95	2.012 → 2.090	2.108 → 1.994
$Lu_3N@C_{80}$		6.93	2.043	
$CeSc_2N@C_{80}$	6.85	6.96	1.946 → 2.047	2.192 → 2.051
$Sc_3N@C_{80}$		6.90	2.025	

[a]IP values are in eV; bond lengths are in Å. [b]The mean M–N bond lengths in CeM_2N clusters are listed.

computed ionization potentials (IPs). Two ionization pathways, $Ce^{III} \rightarrow Ce^{IV}$ (IP_{Ce}) and oxidation of the carbon cage (IP_{cage}), were analyzed. IP_{Ce} was modeled by the singlet state of the $[CeM_2N@C_{80}]^+$ cation, whereas IP_{cage} was addressed by studying the triplet state of $[CeM_2N@C_{80}]^+$.

Computed IPs of $M_3N@C_{80}$ NCFs and IP_{cage} values of $CeM_2N@C_{80}$ are all within the range of 6.90–6.96 eV. Hence, if oxidation of $CeM_2N@C_{80}$ molecules were a cage-based process, similar oxidation potentials might be expected. However, in perfect agreement with electrochemical data, computation shows that removal of the f^1 electron from Ce^{III} is more energetically favorable, that is, IP_{Ce} is lower than IP_{cage} for all $CeM_2N@C_{80}$. Furthermore, IP_{Ce} values show pronounced variation with M (from 6.34 eV in $CeY_2N@C_{80}$ to 6.85 eV in $CeSc_2N@C_{80}$) and follow the same trend as that found in oxidation potentials. The good agreement with experimental electrochemical data enables the use of computations for a more detailed analysis of the role of the second metal presented in the next paragraph. Note that analysis of the redox properties of $CeM_2N@C_{80}$ based on the frontier MO calculations of the neutral molecules would provide erroneous results. As can be seen in Figure 3, the MO with predominant contribution from the Ce-$4f^1$ atomic orbital is 0.84 and 0.37 eV below the cage-based HOMO level in $CeSc_2N@C_{80}$ and $CeLu_2N@C_{80}$, respectively. For $CeY_2N@C_{80}$, the Ce-based MO is mixed

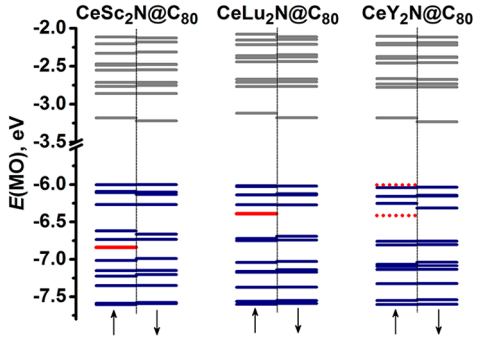

Figure 3. Energy levels of spin-up and spin-down frontier Kohn–Sham molecular orbitals in $CeM_2N@C_{80}$ molecules. Occupied MOs are depicted in blue, unoccupied MOs are in gray, and the occupied MOs with predominant Ce-$4f^1$ contributions are shown in red (for $CeM_2N@C_{80}$, two MOs have approximately equal contributions and are shown with dotted lines).

dx.doi.org/10.1021/jz4009773 | J. Phys. Chem. Lett. 2013, 4, 2404–2409

with two cage MOs (shown in red in Figure 3). On the basis of the MO levels, one might expect the cage-based oxidation in $CeM_2N@C_{80}$ molecules, which contradicts the experimental data. Hence, it is crucial to take into account the changes in the geometry parameters and electronic structure induced by the removal of the electron. However, it will be interesting to see how this situation may affect the electron transport properties of $CeM_2N@C_{80}$ and dynamics of the endohedral cluster (such as recently studied by scanning tunneling microscopy for $Sc_3N@C_{80}$[40,41]) because the localized nature of f electrons usually makes them nonactive in scanning tunneling spectra.

For $CeSc_2N@C_{80}$, DFT predicts a planar $CeSc_2N$ cluster with the Ce−N bond length of 2.192 Å (the exptl. value is 2.184 Å[32]). The Sc−N bond is only 1.946 Å (exptl. 1.933/1.944 Å[32]), considerably shorter than 2.025 Å in $Sc_3N@C_{80}$. When two Sc atoms in $CeSc_2N$ are replaced by Lu with the larger ionic radius, the Ce−N bond is shortened (2.108 Å), and the length of Lu−N bonds (2.012 Å) is decreased compared to that of $Lu_3N@C_{80}$ (2.043 Å). In $CeY_2N@C_{80}$, the Ce−N bond length is further shortened to 2.100 Å, whereas the averaged Y−N bond length, 2.052 Å, is virtually identical to that in $Y_3N@C_{80}$, 2.048 Å. Thus, the C_{80} cage provides a limited interior space, and encapsulation of the large Ce^{3+} ion within the CeM_2N cluster results in a significant strain and shortening of the M−N bonds as compared to their lengths in $M_3N@C_{80}$. Obviously, the strain increases with the ionic radius of M^{3+}. Furthermore, because the cluster in $Y_3N@C_{80}$ is already strongly strained,[42] the Y−N bonds cannot become shorter in $CeY_2N@C_{80}$. To increase the length of the Ce−N bond, the nitrogen atom is displaced above the CeY_2 plane by 0.408 Å, and the CeY_2N cluster becomes pyramidal (Figure 4), similar to Gd_3N in $Gd_3N@C_{80}$.[43]

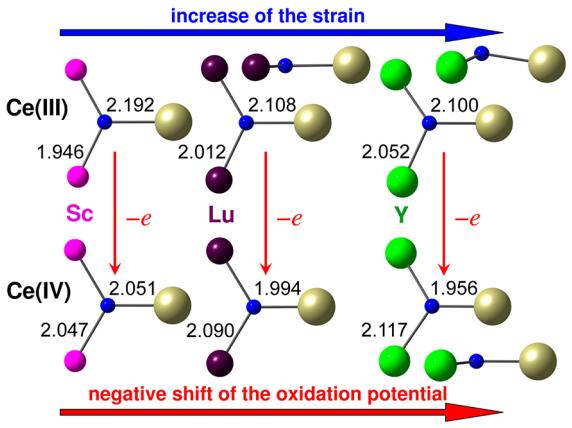

Figure 4. DFT-optimized bond lengths (Å) of the $Ce^{III}M_2N$ and $Ce^{IV}M_2N$ clusters (M = Sc, Y, and Lu) in $CeM_2N@C_{80}$ and $[CeM_2N@C_{80}]^+$, respectively.

When Ce-based oxidation of $CeM_2N@C_{80}$ takes place, the inner strain is reduced because the ionic radius of Ce^{4+} (0.85 Å) is smaller than that of Ce^{3+} (1.03 Å). Hence, Ce−N bonds in $[Ce^{IV}M_2N@C_{80}]^+$ cations are much shorter than those in neutral molecules, whereas M−N bonds are longer (even than those in $M_3N@C_{80}$!). For instance, the Y−N bonds in $[CeY_2N@C_{80}]^+$, 2.117 Å, are longer than those in $Y_3N@C_{80}$, 2.048 Å, whereas the Ce−N bond is as short as 1.956 Å, and the $Ce^{IV}Y_2N$ cluster is planar. The effective radius of Ce^{IV} in NCFs is comparable to that of Sc. Thus, not only is the Ce^{III}-induced strain in the CeM_2N cluster released when Ce is oxidized but also a substitution of one M atom in the M_3N cluster by a small Ce^{4+} releases the strain of the encaged M_3N cluster.

The influence of the strain on the oxidation potential of endohedral Ce^{III} in $CeM_2N@C_{80}$ also explains why endohedral $Ce^{III} \rightarrow Ce^{IV}$ was not observed in many other Ce-based EMFs such as $Ce_2@C_{72,78,80}$,[18−21] $Ce@C_{82}$,[22] or $Ce_3N@C_{88,92,96}$.[23,24] In these molecules, either the number of Ce atoms is too small (mono- and dicerium fullerenes) or the cage size is too large ($Ce_3N@C_{2n}$), resulting in the relatively low inner strain in comparison to Ce-based nitride clusterfullerenes with a C_{80} cage. For instance, DFT calculations for $Ce_3N@C_{88}$ show that its IP_{cage}, 6.26 eV, is smaller than IP_{Ce}, 6.41 eV. Likewise, IP_{cage} of $Ce_2@C_{72}$, 6.47 eV, is also noticeably smaller than IP_{Ce}, 7.06 eV. Hence, oxidation of the carbon cage is more energetically preferable than Ce-based oxidation in these structures.

In summary, we have synthesized $CeY_2N@C_{80}$ and performed an NMR spectroscopic and electrochemical study of a series of $CeM_2N@C_{80}$ NCFs (M = Sc, Lu, Y). The strong support of the endohedral $Ce^{III} \rightarrow Ce^{IV}$ oxidation in these compounds is provided by NMR spectroscopy of the $[CeM_2N@C_{80}]^+$ cations. Although the second cluster metal (Sc, Y, Lu) is not involved in the redox process, the oxidation potential of $CeM_2N@C_{80}$ is a function of the M^{3+} ionic radius and varies in the range of 0.4 V depending on the metal. The large size of the cluster and the limited inner space of the carbon cage result in the inherent strain, and the driving force of the endohedral oxidation of Ce^{III} in $CeM_2N@C_{80}$ is the release of this strain when Ce^{IV} with small ionic radius is formed. Because an increase of the ionic radius of M^{3+} (Sc → Lu → Y) increases the cluster-induced strain, the oxidation potential of $CeM_2N@C_{80}$ shifts to more negative values for larger M^{3+} ions. This is the first discovery of such a relationship between the redox potential of an EMF and the geometry of endohedral species.

■ ASSOCIATED CONTENT

Supporting Information

Details of synthesis, HPLC separation, mass spectrometric characterization, and spectroscopic measurements. This material is available free of charge via the Internet at http://pubs.acs.org.

■ AUTHOR INFORMATION

Corresponding Author

*E-mail: a.popov@ifw-dresden.de (A.A.P.); l.dunsch@ifw-dresden.de (L.D.).

Notes

The authors declare no competing financial interest.

■ ACKNOWLEDGMENTS

Technical assistance of Anja Grohme, B. Urban, M. Rosenkranz, and F. Ziegs (IFW Dresden) is acknowledged. Financial support was provided by DFG (Project PO 1602/1-1) and Chinese Scholar Council (to Y.Zh.). Computations were supported by the Supercomputing Center of Moscow State University.[44]

■ REFERENCES

(1) Popov, A. A.; Yang, S.; Dunsch, L. Endohedral Fullerenes. *Chem. Rev.* **2013**, DOI: 10.1021/cr300297.

(2) Lu, X.; Feng, L.; Akasaka, T.; Nagase, S. Current Status and Future Developments of Endohedral Metallofullerenes. *Chem. Soc. Rev.* **2012**, *41*, 7723−7760.
(3) Rodriguez-Fortea, A.; Balch, A. L.; Poblet, J. M. Endohedral Metallofullerenes: A Unique Host−Guest Association. *Chem. Soc. Rev.* **2011**, *40*, 3551−3563.
(4) Yang, S.; Liu, F.; Chen, C.; Jiao, M.; Wei, T. Fullerenes Encaging Metal Clusters—Clusterfullerenes. *Chem. Commun.* **2011**, *47*, 11822−11839.
(5) Chaur, M. N.; Melin, F.; Ortiz, A. L.; Echegoyen, L. Chemical, Electrochemical, and Structural Properties of Endohedral Metallofullerenes. *Angew. Chem., Int. Ed.* **2009**, *48*, 7514−7538.
(6) Popov, A. A.; Dunsch, L. Electrochemistry in Cavea: Endohedral Redox Reactions of Encaged Species in Fullerenes. *J. Phys. Chem. Lett.* **2011**, *2*, 786−794.
(7) Popov, A. A.; Chen, N.; Pinzón, J. R.; Stevenson, S.; Echegoyen, L. A.; Dunsch, L. Redox-Active Scandium Oxide Cluster Inside a Fullerene Cage: Spectroscopic, Voltammetric, Electron Spin Resonance Spectroelectrochemical, and Extended Density Functional Theory Study of $Sc_4O_2@C_{80}$ and Its Ion Radicals. *J. Am. Chem. Soc.* **2012**, *134*, 19607−19618.
(8) Zhang, L.; Popov, A. A.; Yang, S.; Klod, S.; Rapta, P.; Dunsch, L. An Endohedral Redox System in a Fullerene Cage: The Ce Based Mixed Cluster Fullerene $Lu_2CeN@C_{80}$. *Phys. Chem. Chem. Phys.* **2010**, *12*, 7840−7847.
(9) Chen, C.; Liu, F.; Li, S.; Wang, N.; Popov, A. A.; Jiao, M.; Wei, T.; Li, Q.; Dunsch, L.; Yang, S. Titanium/Yttrium Mixed Metal Nitride Clusterfullerene $TiY_2N@C_{80}$: Synthesis, Isolation, and Effect of the Group-III Metal. *Inorg. Chem.* **2012**, *51*, 3039−3045.
(10) Popov, A. A.; Chen, C.; Yang, S.; Lipps, F.; Dunsch, L. Spin-Flow Vibrational Spectroscopy of Molecules with Flexible Spin Density: Electrochemistry, ESR, Cluster and Spin Dynamics, and Bonding in $TiSc_2N@C_{80}$. *ACS Nano* **2010**, *4*, 4857−4871.
(11) Yang, S.; Chen, C.; Popov, A.; Zhang, W.; Liu, F.; Dunsch, L. An Endohedral Titanium(III) in a Clusterfullerene: Putting a Non-Group-III Metal Nitride into the C_{80}-I_h Fullerene Cage. *Chem. Commun.* **2009**, 6391−6393.
(12) Dunsch, L.; Yang, S. Metal Nitride Cluster Fullerenes: Their Current State and Future Prospects. *Small* **2007**, *3*, 1298−1320.
(13) Stevenson, S.; Rice, G.; Glass, T.; Harich, K.; Cromer, F.; Jordan, M. R.; Craft, J.; Hadju, E.; Bible, R.; Olmstead, M. M.; et al. Small-Bandgap Endohedral Metallofullerenes in High Yield and Purity. *Nature* **1999**, *401*, 55−57.
(14) Yang, S. F.; Zalibera, M.; Rapta, P.; Dunsch, L. Charge-Induced Reversible Rearrangement of Endohedral Fullerenes: Electrochemistry of Tridysprosium Nitride Clusterfullerenes $Dy_3N@C_{2n}$ (2n=78, 80). *Chem.—Eur. J.* **2006**, *12*, 7848−7855.
(15) Cardona, C. M.; Elliott, B.; Echegoyen, L. Unexpected Chemical and Electrochemical Properties of $M_3N@C_{80}$ (M = Sc, Y, Er). *J. Am. Chem. Soc.* **2006**, *128*, 6480−6485.
(16) Valencia, R.; Rodriguez-Fortea, A.; Clotet, A.; de Graaf, C.; Chaur, M. N.; Echegoyen, L.; Poblet, J. M. Electronic Structure and Redox Properties of Metal Nitride Endohedral Fullerenes $M_3N@C_{2n}$ (M=Sc, Y, La, and Gd; 2n=80, 84, 88, 92, 96). *Chem.—Eur. J.* **2009**, *15*, 10997−11009.
(17) Popov, A. A.; Dunsch, L. Hindered Cluster Rotation and ^{45}Sc Hyperfine Splitting Constant in Distonoid Anion Radical $Sc_3N@C_{80}$, and Spatial Spin Charge Separation as a General Principle for Anions of Endohedral Fullerenes with Metal-Localized Lowest Unoccupied Molecular Orbitals. *J. Am. Chem. Soc.* **2008**, *130*, 17726−17742.
(18) Yamada, M.; Mizorogi, N.; Tsuchiya, T.; Akasaka, T.; Nagase, S. Synthesis and Characterization of the D_{5h} Isomer of the Endohedral Dimetallofullerene $Ce_2@C_{80}$: Two-Dimensional Circulation of Encapsulated Metal Atoms Inside a Fullerene Cage. *Chem.—Eur. J.* **2009**, *15*, 9486−9493.
(19) Yamada, M.; Nakahodo, T.; Wakahara, T.; Tsuchiya, T.; Maeda, Y.; Akasaka, T.; Kako, M.; Yoza, K.; Horn, E.; Mizorogi, N.; et al. Positional Control of Encapsulated Atoms Inside a Fullerene Cage by Exohedral Addition. *J. Am. Chem. Soc.* **2005**, *127*, 14570−14571.
(20) Yamada, M.; Wakahara, T.; Tsuchiya, T.; Maeda, Y.; Kako, M.; Akasaka, T.; Yoza, K.; Horn, E.; Mizorogi, N.; Nagase, S. Location of the Metal Atoms in $Ce_2@C_{78}$ and Its Bis-Silylated Derivative. *Chem. Commun.* **2008**, 558−560.
(21) Yamada, M.; Wakahara, T.; Tsuchiya, T.; Maeda, Y.; Akasaka, T.; Mizorogi, N.; Nagase, S. Spectroscopic and Theoretical Study of Endohedral Dimetallofullerene Having a Non-IPR Fullerene Cage: $Ce_2@C_{72}$. *J. Phys. Chem. A* **2008**, *112*, 7627−7631.
(22) Suzuki, T.; Kikuchi, K.; Oguri, F.; Nakao, Y.; Suzuki, S.; Achiba, Y.; Yamamoto, K.; Funasaka, H.; Takahashi, T. Electrochemical Properties of Fullerenolanthanides. *Tetrahedron* **1996**, *52*, 4973−4982.
(23) Chaur, M. N.; Melin, F.; Elliott, B.; Kumbhar, A.; Athans, A. J.; Echegoyen, L. New $M_3N@C_{2n}$ Endohedral Metallofullerene Families (M=Nd, Pr, Ce; n=40−53): Expanding the Preferential Templating of the C_{88} Cage and Approaching the C_{96} Cage. *Chem.—Eur. J.* **2008**, *14*, 4594−4599.
(24) Chaur, M. N.; Melin, F.; Ashby, J.; Kumbhar, A.; Rao, A. M.; Echegoyen, L. Lanthanum Nitride Endohedral Fullerenes $La_3N@C_{2n}$ ($43 < n < 55$): Preferential Formation of $La_3N@C_{96}$. *Chem.—Eur. J.* **2008**, *14*, 8213−8219.
(25) Sroor, F. M. A.; Edelmann, F. T. Tetravalent Cerium Chemistry. In *Cerium: Molecular Structure, Technological Applications and Health Effects*; Izyumov, A., Plaksin, G., Eds.; Nova Science Publishers: Hauppauge, New York, 2012.
(26) Streitwieser, A. J.; Kinsley, S. A.; Rigsbee, J. T.; Fragala, I. L.; Ciliberto, E. Photoelectron Spectra And Bonding In Cerocene, Bis(π-[8]annulene)cerium(IV). *J. Am. Chem. Soc.* **1985**, *107*, 7786−7788.
(27) Gulino, A.; Casarin, M.; Conticello, V. P.; Gaudiello, J. G.; Mauermann, H.; Fragala, I.; Marks, T. J. Efficient Synthesis, Redox Characteristics, and Electronic Structure of a Tetravalent Tris(cyclopentadienyl)cerium Alkoxide Complex. *Organometallics* **1988**, *7*, 2360−2364.
(28) Buchler, J. W.; Scharbert, B. Metal Complexes with Tetrapyrrole Ligands. 50. Redox Potentials of Sandwichlike Metal Bis(octaethylporphyrinates) and Their Correlation with Ring−Ring Distances. *J. Am. Chem. Soc.* **1988**, *110*, 4272−4276.
(29) Robinson, J. R.; Carroll, P. J.; Walsh, P. J.; Schelter, E. J. The Impact of Ligand Reorganization on Cerium(III) Oxidation Chemistry. *Angew. Chem., Int. Ed.* **2012**, *51*, 10159−10163.
(30) Schelter, E. J. Cerium under the Lens. *Nat. Chem.* **2013**, *5*, 348.
(31) Yang, S.; Zhang, L.; Zhang, W.; Dunsch, L. A Facile Route to Metal Nitride Clusterfullerenes by Using Guanidinium Salts: A Selective Organic Solid as the Nitrogen Source. *Chem.—Eur. J.* **2010**, *16*, 12398−12405.
(32) Wang, X. L.; Zuo, T. M.; Olmstead, M. M.; Duchamp, J. C.; Glass, T. E.; Cromer, F.; Balch, A. L.; Dorn, H. C. Preparation and Structure of $CeSc_2N@C_{80}$: An Icosahedral Carbon Cage Enclosing an Acentric $CeSc_2N$ Unit with Buried f Electron Spin. *J. Am. Chem. Soc.* **2006**, *128*, 8884−8889.
(33) Yang, S.; Popov, A. A.; Dunsch, L. Carbon Pyramidalization in Fullerene Cages Induced by the Endohedral Cluster: Non-Scandium Mixed Metal Nitride Clusterfullerenes. *Angew. Chem., Int. Ed.* **2008**, *47*, 8196−8200.
(34) Greenwood, N. N.; Earnshaw, A. *Chemistry of the Elements*; Pergamon: Oxford, U.K., 1984.
(35) Haddon, R. C. Pyramidalization — Geometrical Interpretation of the π-Orbital Axis Vector in 3 Dimensions. *J. Phys. Chem.* **1987**, *91*, 3719−3720.
(36) Elliott, B.; Yu, L.; Echegoyen, L. A Simple Isomeric Separation of D_{5h} and I_h $Sc_3N@C_{80}$ by Selective Chemical Oxidation. *J. Am. Chem. Soc.* **2005**, *127*, 10885−10888.
(37) Tarabek, J.; Yang, S.; Dunsch, L. Redox Properties of Mixed Lutetium/Yttrium Nitride Clusterfullerenes: Endohedral $Lu_xY_{3-x}N@C_{80}$(I) (x=0−3) Compounds. *ChemPhysChem* **2009**, *10*, 1037−1043.
(38) Connelly, N. G.; Geiger, W. E. Chemical Redox Agents for Organometallic Chemistry. *Chem. Rev.* **1996**, *96*, 877−910.
(39) Granovsky, A. A. *Firefly*, version 8.0.0. http://classic.chem.msu.su/gran/firefly/index.html (2008).

(40) Huang, T.; Zhao, J.; Feng, M.; Popov, A. A.; Yang, S.; Dunsch, L.; Petek, H. A Multi-State Single-Molecule Switch Actuated by Rotation of an Encapsulated Cluster within a Fullerene Cage. *Chem. Phys. Lett.* **2012**, *552*, 1−12.
(41) Huang, T.; Zhao, J.; Feng, M.; Popov, A. A.; Yang, S.; Dunsch, L.; Petek, H. A Molecular Switch Based on Current-Driven Rotation of an Encapsulated Cluster within a Fullerene Cage. *Nano Lett.* **2011**, *11*, 5327−5332.
(42) Popov, A. A. Metal-Cage Bonding, Molecular Structures and Vibrational Spectra of Endohedral Fullerenes: Bridging Experiment and Theory. *J. Comput. Theor. Nanosci.* **2009**, *6*, 292−317.
(43) Stevenson, S.; Phillips, J. P.; Reid, J. E.; Olmstead, M. M.; Rath, S. P.; Balch, A. L. Pyramidalization of Gd_3N Inside a C_{80} cage. The Synthesis and Structure of $Gd_3N@C_{80}$. *Chem. Commun.* **2004**, 2814−2815.
(44) Voevodin, V. V.; Zhumatiy, S. A.; Sobolev, S. I.; Antonov, A. S.; Bryzgalov, P. A.; Nikitenko, D. A.; Stefanov, K. S.; Voevodin, V. V. Practice of "Lomonosov" Supercomputer. *Open Systems J.* [Online]. http://www.osp.ru/os/2012/07/13017641 (2012).